Dopamine Cells Differentially Regulate Striatal Cholinergic Transmission across Regions through Corelease of Dopamine and Glutamate

Yuan Cai[1,2]Christopher P. Ford[1,2,3,*]

[1]Department of Pharmacology, University of Colorado School of Medicine, Anschutz Medical Campus, Aurora, CO 80045, USA

[2]Department of Physiology and Biophysics, Case Western Reserve University School of Medicine, Cleveland, OH 44106, USA

[3]Lead Contact

SUMMARY

The balance of dopamine and acetylcholine in the dorsal striatum is critical for motor and learning functions. Midbrain dopamine cells and local cholinergic interneurons (ChIs) densely innervate the striatum and have strong reciprocal actions on each other. Although dopamine inputs regulate ChIs, the functional consequences of dopamine neuron activity across dorsal striatal regions is poorly understood. Here, we find that midbrain dopamine neurons drive pauses in the firing of dorsomedial ChIs but robust bursts in dorsolateral ChIs. Pauses are mediated by dopamine D2 receptors, while bursts are driven by glutamate corelease and activation of a mGluR-mediated excitatory conductance. We find the frequency of muscarinic cholinergic transmission to medium spiny neurons is greater in the dorsomedial striatum. This regional variation in transmission is moderated by the different actions of dopamine and glutamate corelease. These results delineate a mechanism by which dopamine inputs maintain consistent levels of cholinergic activity across the dorsal striatum.

Graphical Abstract

*Correspondence: christopher.ford@ucdenver.edu.

AUTHOR CONTRIBUTIONS

Y.C. and C.P.F. designed and performed experiments, analyzed the data, and wrote the manuscript.

DECLARATION OF INTERESTS

The authors declare no competing interests.
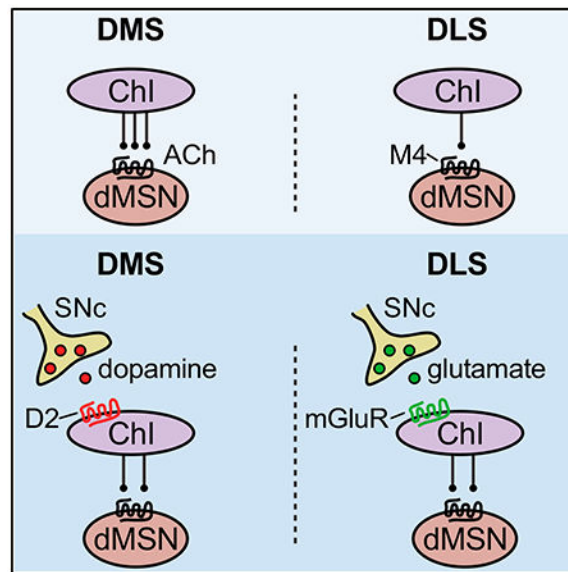
In Brief

Cai and Ford identify regional differences in the extent of ACh transmission onto direct pathway medium spiny neurons between the dorsomedial and the dorsolateral striatum. These differences were normalized by SNc inputs, which had opposing actions on the firing of cholinergic interneurons in each region.

INTRODUCTION

The dorsal striatum integrates excitatory inputs from various brain regions with modulatory inputs from dopamine neurons in the substantia nigra pars compacta (SNc), as well as cholinergic interneurons (ChIs) within the striatum (Bolam et al., 2000; Calabresi et al., 2000; Gerfen and Wilson, 1996; Kreitzer, 2009). It is widely recognized that dopaminergic and cholinergic neurons functionally cooperate with each other, and their interactions are critical for motivated behaviors and locomotion (Aosaki et al., 2010; Pisani et al., 2007). Synchronous firing of ChIs drives dopamine release from dopamine terminals via presynaptic nicotinic receptors (Cachope et al., 2012; Threlfell et al., 2012), whereas dopamine cells primarily inhibit ChIs via dopamine D2 receptors (Aosaki et al., 1994a; Chuhma et al., 2014; Gerfen and Surmeier, 2011; Graybiel et al., 1994; Morris et al., 2004). Studies have found that optogenetic activation of dopamine inputs mainly inhibits dorsal striatal cholinergic activity through dopamine D2 receptors but can also lead to a transient excitation in a subset of cells (Chuhma et al., 2014; Straub et al., 2014). However, the mechanisms and functional consequences of this modulation remain unclear.

The dorsal striatum can be anatomically and functionally separated into the dorsomedial striatum (DMS) and the dorsolateral striatum (DLS) (Gremel and Costa, 2013; Kupferschmidt et al., 2017; McGeorge and Faull, 1989; Yin and Knowlton, 2006). Each region receives largely different dopamine inputs (Lerner et al., 2015), and past work has shown that the DMS is associated with goal-directed behaviors (Devan et al., 1999; Yin et

al., 2005), while the DLS is responsible for habit formation and locomotion (West et al., 1990; Yin and Knowlton, 2006; Yin et al., 2004). Although ChIs are thought to be a relatively homogeneous population of cells, it is unclear whether cholinergic transmission differs across the DMS and the DLS and whether transmission is modulated differently by dopamine across regions. Here we compared cholinergic transmission between the DMS and the DLS and examined effects of dopamine inputs across these two regions in striatal slices. We found that basal cholinergic transmission during tonic ChI activity is higher in the DMS than the DLS. Optogenetic activation of dopamine inputs differentially altered cholinergic transmission across these regions via anatomically distinct patterns of dopamine-glutamate cotransmission. The net effect was an inhibition of cholinergic transmission in the DMS but a facilitation in the DLS. These findings highlight the regional specificity of dopamine-acetylcholine interaction in the dorsal striatum, which might contribute to distinct behavioral outcomes when sub-striatal regions are separately recruited.

RESULTS

Dopamine Inputs Differentially Modulate Cholinergic Activity in the DMS and DLS

To examine how dopamine inputs modulate striatal ChI firing, an adeno-associated virus (AAV) encoding double-floxed channelr-hodopsin 2 (ChR2) and enhanced yellow fluorescent protein (EYFP) was injected into the midbrain of mice expressing Cre recombinase under the dopamine transporter (DAT) promoter (Figure 1A). After allowing three weeks for viral expression, we observed broad expression of EYFP in the substantia nigra pars compacta (SNc), as well as in the striatum (Figure 1B). We performed cell-attached recordings of ChIs in coronal striatal slices. ChIs were initially targeted using their large soma size, and the identity of ChIs was confirmed by the presence of tonic pacemaker firing and by re-patching cells in whole-cell configuration at the end of the experiment to verify the presence of a hyperpolarization-evoked inward current (I_h) (Kawaguchi, 1993). In half of ChIs, optogenetic stimulation of dopaminergic inputs (5 pulses at 20 Hz, 2 ms each) led to a pause in spontaneous firing, which was eliminated following application of the D2 receptor antagonist sulpiride (500 nM) (average firing frequency 1 s following flash: control, 0.3 ± 0.1 Hz; sulpiride, 1.5 ± 0.5 Hz; n = 10/20, p < 0.01, Wilcoxon test) (Figure 1C, left). This is consistent with the previous findings that dopamine inhibits cholinergic activity through D2 receptors (Aosaki et al., 1994a; Chuhma et al., 2014). In the other half of ChIs, we found that instead of evoking a pause in firing, photoactivation of dopaminergic inputs drove a brief pause (average firing frequency: baseline, 1.5 ± 0.5 Hz; 200 ms following flash, 0 Hz; n = 10/20, p < 0.01, Wilcoxon test) (Figure S1) that was followed by a burst of action potentials (n = 10), which lasted approximately 1 s (Figure 1C, right). The short pause was diminished by the D2 receptor antagonist sulpiride (500 nM) (average firing frequency: baseline, 1.5 ± 0.5 Hz; 200 ms following flash in sulpiride, 1.9 ± 1.8 Hz; n = 10, p > 0.05, Wilcoxon test) (Figure S1), but the burst was unaffected (average firing frequency 1 s following flash: control, 8.1 ± 1.9 Hz; sulpiride, 6.9 ± 1.4 Hz; n = 10, p > 0.05, Wilcoxon test) (Figure 1C, right). The lag until onset of bursting varied between 240 and 649 ms (average, 443 ± 52 ms) following the flash, and the extent of the burst firing was graded with the intensity of photostimulation (Figure S1).

In the presence of sulpiride (500 nM), we found that ChIs could be classified into three types based on their response to activation of dopaminergic inputs, with a third failing to respond (type 1; n = 40, p > 0.05, Wilcoxon test), a third showing a slight increase in firing (type 2, 3.5-fold increase; n = 36, p < 0.0001, Wilcoxon test), and a third exhibiting a robust burst of action potentials (type 3, 16-fold increase; n = 44, p < 0.0001, Wilcoxon test) (Figure 1D). In the absence of sulpiride, we confirmed that type 1 ChIs exhibited a pause in firing following the dopamine terminal stimulation (Figure S1). Cluster analysis revealed that although type 2 and type 3 ChIs had similar spontaneous baseline firing frequencies, they could be segregated based on the extent of burst firing (Figure 1E). To test whether the different burst responses resulted from differences in their intrinsic excitabilities, we used whole-cell current-clamp recordings to examine the number of action potentials in each ChI type following current injection (100–400 pA, 500 ms). We found that the excitability of type 2 ChIs was greater than that of type 1 ChIs but was similar to that of type 3 ChIs (type 1: 5.2 ± 0.5 action potentials [APs], n = 8; type 2: 7.3 ± 0.6 APs, n = 9; type 3: 6.8 ± 0.5 APs, n = 5; p < 0.05 type 1 versus types 2 and 3, one-way ANOVA Kruskal-Wallis; 300 pA), and there was no difference in input resistance among types (Figures 1F and S1). The similarity between type 2 and type 3 ChIs suggests that intrinsic excitability may not account for the observed differences in ChI responses.

Overlapping populations of dopamine neurons with different properties and encoding different motivational stimuli project to the DMS and DLS (Lerner et al., 2015). To examine how dopamine inputs modulate cholinergic activity in the DMS and DLS, we examined the responses of ChIs in each region. In the presence of sulpiride (500 nM), some ChIs showed a slight increase in firing, but most did not. This resulted in no change in the overall firing rate of DMS ChIs following dopamine terminal stimulation (p > 0.05, n = 28, Wilcoxon test). In contrast, ChIs in the DLS exhibited a strong burst of action potentials (15.8-± 3.3-fold increase; p < 0.0001 versus baseline, n = 51, Wilcoxon test). Classification of ChIs according to their location revealed that 65% of ChIs in the DMS did not respond to dopamine terminal stimulation (type 1, n = 19/29), while 35% showed a slight increase (type 2, n = 10/29) (Figure 1G). This differed from the DLS, in which 62% of ChIs exhibited a burst (type 3, n = 36/58), while only 14% failed to respond (type 1, n = 8/58) (Figure 1G). Altogether, this suggests that dopamine inputs differentially regulate cholinergic activity across the striatum by driving pauses in DMS ChIs but bursts in DLS ChIs.

Corelease of Glutamate from Dopamine Cells Activates an Excitatory mGluR-Mediated Excitatory Conductance in DLS ChIs

Previous work has found that dopamine inputs to the dorsal striatum evoke a D2 receptor-mediated pause in most ChIs and a 1.5- to 3-fold increase in firing rate in a subset of ChIs (Chuhma et al., 2014; Straub et al., 2014). However, the mechanisms underlying the increase in dorsal striatum ChI activity are not known (Straub et al., 2014). One possibility is the activation of excitatory D1-like dopaminergic receptors on ChIs. ChIs express D5 dopamine receptors (Bergson et al., 1995; Yan and Surmeier, 1997), which are members of the D1-like receptor family. Stimulation of these receptors increases ChI activity in striatal slices (Aosaki et al., 1998). However, inhibition of D1/D5 receptors with SCH23390 (1 µM) did not alter SNc-driven ChI bursting in type 2 or type 3 ChIs (Figures 2A and 2B). Work has

determined that dopamine neurons corelease multiple neurotransmitters, including γ-aminobutyric acid (GABA) and glutamate (Hnasko et al., 2010; Nelson et al., 2014; Stuber et al., 2010; Tritsch et al., 2012). Dopamine neuron cotransmission varies across striatal subregions, and in the nucleus accumbens, the corelease of glutamate evokes AMPA and NMDA synaptic events in both medium spiny neurons (MSNs) and ChIs (Chuhma et al., 2014, 2017; Stuber et al., 2010). To test whether coreleased GABA or glutamate drives DLS ChI bursting, we blocked AMPA, NMDA, or GABA receptors. However, application of DNQX (10 μM), AP5 (10 μM), picrotoxin (100 μM), or CGP55845 (300 nM) did not alter the burst response of DLS ChIs (control, 13.1 ± 2.7 Hz; picrotoxin and CGP, 13.3 ± 3.9 Hz; DNQX and AP5, 11.8 ± 2.6 Hz; $p > 0.05$, Kruskal-Wallis test) (Figures 2A and 2B).

In addition to ligand-gated glutamatergic receptors, ChIs express G_q-coupled group 1 metabotropic glutamate receptors (mGluRs) (Lim et al., 2014; Tallaksen-Greene et al., 1998), and agonists of these receptors depolarize striatal ChIs (Bonsi et al., 2005; Pisani et al., 2001). Thus, it is possible that corelease of glutamate from dopamine terminals might be able to act on mGluRs to drive ChI facilitation. Application of group I mGluR antagonists MPEP (100 μM) and CPCCOEt (100 μM) did not alter the baseline firing of ChIs (control, 0.9 ± 0.3 Hz; antagonists, 0.6 ± 0.2 Hz; $n = 8$, $p > 0.05$, Wilcoxon test), but it eliminated DLS ChI bursting induced by activation of dopaminergic inputs (control, 14.2 ± 3 Hz; antagonists, 1.4 ± 0.7 Hz; $n = 8$, $p < 0.01$, Wilcoxon test) (Figure 2C). These findings suggest that glutamate released from dopamine terminals drives firing in DLS ChIs by activating group I mGluRs.

We next examined the signaling cascade downstream of mGluRs that underlies ChI bursting. We performed cell-attached and whole-cell voltage-clamp recordings sequentially in the same ChI while activating dopamine terminals (Figure 3A). Similar to previous studies (Straub et al., 2014), we found that photoactivation of dopamine terminals evoked an inward current in ChIs (Figure 3B). The amplitude of the inward current correlated with the extent of bursting in ChIs across the dorsal striatum ($r = 0.72$, $p < 0.001$, Pearson's correlation) (Figure 3C). Then we focused on type 3 ChIs in the DLS with the aim of understanding this depolarizing conductance. The group I mGluR1 antagonists MPEP (100 uM) and CPCCOEt (100 μM) eliminated the inward current (control, 72.2 ± 15.2 pA; antagonists, 8.9 ± 3.9 pA; $n = 7$, $p < 0.05$, Wilcoxon test) (Figures 3D and 3E), confirming that it was driven by glutamate transmission. The inward current was also blocked by TTX (200 nM) (control, 38.0 ± 7.1 pA; antagonists, 2.9 ± 0.7 pA; $n = 7$, $p < 0.05$, Wilcoxon test) (Figure 3F). Dialysis of ChIs with either intracellular GDPβS (0.6 mM), a non-hydrolysable analog of guanosine diphosphate (GDP) that inhibits G-protein signaling (control, 25.7 ± 6.9 pA, $n = 7$; GDPβS, 5.2 ± 1 pA, $n = 14$; $p < 0.001$, Mann-Whitney test) (Figures 3G and 3H) or intracellular BAPTA (10 mM) (control, 23.6 ± 5.5 pA, $n = 10$; GDPβS, 8.3 ± 2.8 pA, $n = 5$; $p < 0.05$, Mann-Whitney test) (Figure 3I) decreased the inward current, indicating that the excitatory current in DLS ChIs is the result of G-protein-driven intracellular calcium signaling. Current-voltage analysis showed that the inward current had a reversal potential near +10 mV, suggestive of a non-selective cation ion conductance (Figure 3J). Striatal ChIs express various types of transient receptor potential C (TrpC) channels, which are non-selective ion channels commonly activated downstream of group I mGluRs (Berg et al., 2007; El-Hassar et al., 2011). We found that dopamine neuron-induced bursts in ChIs were

eliminated by application of clemizole (10 μM) (control, 12.5 ± 1.8 Hz; clemizole, 1.2 ± 0.4 Hz; n = 7, p < 0.05, Wilcoxon test) (Figure 3K) or M 084 (100 μM) (control, 12.4 ± 2 Hz; M 084, 2.6 ± 1 Hz; n = 10, p < 0.01, Wilcoxon test) (Figure 3L), compounds known to block TrpC channels. Altogether, this suggests that the corelease of glutamate evokes bursts in a subset of ChIs through the activation of a mGluR-mediated excitatory conductance likely mediated by Trp channels.

Differences in Glutamate Corelease and D2 Receptor Signaling across ChIs

Our results suggest that activation of SNc dopamine terminals primarily drives pauses in DMS ChIs but bursts in DLS ChIs. This could be due to either postsynaptic differences in D2 or mGluR signaling among ChIs or presynaptic differences in the extent of dopamine-glutamate corelease from midbrain dopamine terminals innervating each region. To address this, we directly applied either dopamine (1 M) or L-aspartate (200 mM, in the presence of AMPA and NMDA blockers) to ChIs via iontophoresis. We found that application of dopamine (1 M, 50 ms) robustly drove pauses in ChI firing in DMS ChIs (baseline, 1.4 ± 0.2 Hz; dopamine [DA], 0.1 ± 0.1 Hz; n = 10, p < 0. 01, Wilcoxon test) but was more variable and less robust in DLS ChIs (baseline, 1.3 ± 0.2 Hz; DA, 0.8 ± 0.3 Hz; n = 10, p < 0.05, Wilcoxon test) (Figures 4A and 4B). In both cases, the effect of dopamine was blocked by the D2-antagonist sulpiride (500 nM) (Figure 4A). Thus, dopamine is less effective in driving D2 receptor-mediated pauses in DLS ChIs. This result suggests that the difference in dopamine responses of DMS and DLS ChIs is due to post-synaptic differences in the extent of D2 receptor-mediated inhibition.

In contrast, application of L-aspartate (200 mM, 50 ms) drove bursting equally effectively in both type 1 DMS ChIs (baseline, 1.2 ± 0.3 Hz; aspartate [Asp], 3.2 ± 0.8 Hz; n = 9, p < 0.01, Wilcoxon test) and type 3 DLS ChIs (baseline, 1.1 ± 0.3 Hz; Asp, 4.3 ± 1.5 Hz; n = 9, p < 0.01, Wilcoxon test) (Figures 4C and 4D). The effect of L-aspartate in both regions was blocked by the group I mGluR antagonists MPEP (100 μM) and CPCCOEt (100 μM) (Figure 4C). This suggests that mGluRs couple equally effectively to their excitatory channels across both DMS and DLS ChIs. Because direct activation mGluRs drives bursting in all ChIs, but activation of SNc axons in the DMS does so only weakly in some ChIs, our results suggest that the extent of glutamate corelease onto ChIs from SNc terminals in the DMS is weaker than in the DLS.

Regional Differences in Cholinergic Connectivity and Transmission at Muscarinic Synapses across the Striatum

The release of acetylcholine (ACh) from ChIs regulates striatal activity by presynaptic modulation of dopamine and GABA inputs to MSNs via nicotinic ACh receptors (nAChRs) and muscarinic receptors (Cachope et al., 2012; English et al., 2011; Mamaligas et al., 2016; Threlfell et al., 2012), as well as the activity of MSNs directly via muscarinic receptors (Goldberg et al., 2012). We next examined how dopamine SNc input-driven changes in ChI firing regulate cholinergic transmission across the dorsal striatum. While G_q-coupled M1 mAChRs are expressed in all MSNs, $G_{i/o}$-coupled M4 mAChRs are expressed predominantly in direct pathway MSNs (dMSNs) (Bernard et al., 1992; Goldberg et al., 2012; Lim et al., 2014; Yan et al., 2001). ChIs make monosynaptic connections with dMSNs

at muscarinic M4 receptor-containing synapses (Mamaligas and Ford, 2016). To measure the synaptic activation of M4 receptors on dMSNs, we virally overexpressed a G protein-coupled inwardly rectifying potassium channel (GIRK2, $Kir_{3.2}$) in MSNs. These channels couple to endogenous M4 receptors allowing for an electrophysiological readout of synaptic muscarinic receptor activation (Mamaligas and Ford, 2016). An AAV encoding both GIRK2 and a soluble tdTomato fluorophore under a synapsin promoter was injected into the DMS and the DLS (Figure 5A). The synapsin promoter allows for robust expression in MSNs but restricts expression from ChIs (Mamaligas and Ford, 2016). As such, we found that the properties and excitability of ChIs were similar in AAV-GIRK2-injected animals and uninjected controls (Figure S2).

ChI pacemaker firing drives the release of ACh, which evokes spontaneous muscarinic M4 inhibitory post-synaptic currents (M4-IPSCs) in GIRK2-expressing dMSNs (Mamaligas and Ford, 2016). We recorded spontaneous M4-IPSCs in dMSNs in both the DMS and the DLS (Figure 5B). In both regions, spontaneous M4-IPSCs were blocked by the muscarinic antagonist scopolamine (500 nM) (Figure 5B). The amplitude of spontaneous M4-IPSCs in each region was identical (DMS: 38.9 ± 3.5 pA, n = 14; DLS: 35.1 ± 4.1 pA, n = 13; p > 0.05, Mann-Whitney test), indicating that the level of GIRK expressed in DMS and DLS dMSNs as a result of AAV-mediated expression was the same (Marcott et al., 2014). However, the frequency of events was higher in DMS dMSNs than DLS dMSNs (DMS: 2.8 ± 0.2 Hz, n = 15; DLS: 1.5 ± 0.2 Hz, n = 14; p < 0.001, Mann-Whitney test) (Figure 5C). We also analyzed the area under the curve (AUC) of M4-IPSCs for each trace, and the averaged AUC of a cell was greater in DMS dMSNs than DLS dMSNs (average AUC^{-s}) (DMS: 15.1 ± 1.6 pA*s, n = 15; DLS: 6.8 ± 1.1 pA*s, n = 14; p < 0.001, Mann-Whitney test) (data not shown). The density of ChIs was the same across the dorsal striatum (DMS: 56.9 ± 18.5 $ChIs/mm^2$, n = 3 mice; DLS: 54.8 ± 13.5 $ChIs/mm^2$, n = 3 mice; widefield fluorescence, p > 0.05, Wilcoxon test) (Figures 5D and 5E), suggesting that the higher frequency of IPSCs in the DMS was not due to a greater number of ChIs. We next tested whether the connectivity between ChIs and dMSNs was different across these two regions. We made paired recordings from ChIs (cell attached) and synaptically coupled dMSNs (voltage clamp). In this configuration, both unitary M4-IPSCs that are time locked to the firing of a given ChI (paired IPSCs) and unpaired M4-IPSCs resulting from the firing of other ChIs (unpaired IPSCs) can be observed (Mamaligas and Ford, 2016). In the DMS, we found that of the total M4-IPSCs, 33% were paired while 67% were unpaired (n = 7) (Figure 5G). Because roughly one-third of spontaneous inhibitory postsynaptic currents (sIPSCs) recorded could be attributed to the paired ChI (Figure 5C), it suggests that possibly three ChIs were synaptically coupled to that MSN. This differed from the DLS, in which half of all spontaneous M4-IPSCs were paired (n = 7 pairs, p < 0.05, Mann-Whitney test) (Figure 5G). We calculated the connectivity of ChIs to each dMSN by taking the ratio of the total number of spontaneous M4-IPSCs over the number of paired M4-IPSCs. The ratio was greater in the DMS (DMS: 3.6 ± 0.5, n = 8; DLS: 2.1 ± 0.2, n = 7 pairs; p < 0.05, Mann-Whitney test) (Figure 5H) and suggests that between three and four ChIs are coupled to a given dMSN in the DMS, while only two ChIs may be coupled to dMSN in the DLS. Thus, DMS MSNs have more ChIs coupled to them than do DLS MSNs. In addition, we found that the spontaneous firing rate in DMS ChIs was slightly higher than in DLS ChIs (DMS: 1.5 ± 0.1

Hz, n = 48; DLS: 1.1 ± 0.1 Hz, n = 109; p < 0.05, Mann-Whitney test) (data not shown). Altogether, these results show that as a result of higher ChI firing rates and synaptic convergence, the basal level of cholinergic transmission onto dMSNs is higher in the DMS than the DLS.

Midbrain Dopamine Inputs Use Corelease to Differently Regulate Cholinergic Transmission across Striatal Regions

To examine how midbrain dopamine neuron inputs regulate cholinergic transmission across the DMS and DLS, we next expressed ChR2 in SNc dopamine cells in AAV-GIRK-injected mice and recorded from GIRK2$^+$ dMSNs in each region. Because overlapping spontaneous IPSCs are difficult to identify when the frequency of events is high, we analyzed the AUC of M4-IPSCs for each cell. Photostimulation of dopamine terminals led to a pause in spontaneous M4-IPSCs in DMS dMSNs (average AUC^{-s} 1 s following flash, 52.9% ± 16% of the baseline; p < 0.05, n = 8, Wilcoxon test) but evoked a burst of M4-IPSCs in dMSNs in the DLS (average AUC^{-s} 1 s following flash, 938.0% ± 240% of the baseline; p <0.01, n = 10, Wilcoxon test) (Figure 6A). Thus, like the firing of ChIs, the predominant effect of midbrain dopamine terminal inputs on cholinergic transmission across the striatum is inhibitory in the DMS but excitatory in the DLS. This suggests that nigrostriatal inputs diminish the regional imbalance in basal cholinergic transmission across the dorsal striatum through different combinations of neuromodulation.

To determine the role of dopamine and glutamate in driving these changes in cholinergic transmission, we first applied the D2 receptor antagonist sulpiride. Sulpiride (500 nM) eliminated the pause in M4-IPSCs in the DMS to reveal an underlying potentiation (AUC^{-s} post-flash: control, 52.9% ± 15.9% of baseline; sulpiride [sulp.], 543.7% ± 114.8%; p < 0.01, n = 8, Wilcoxon test). In the DLS, sulpiride (500 nM) induced only a slight potentiation of muscarinic M4-IPSCs (AUC^{-s} post-flash: control, 938.0% ± 240.0% of baseline; sulp., 1367.0% ± 344.1%; p < 0.05, n = 10, Wilcoxon test) (Figures 6B and 6C, red). This confirms the stronger effect of dopamine D2 receptor-mediated inhibition in the DMS. Furthermore, the results indicate that, likely as a result of convergence of both type 1 and type 2 ChIs onto dMSNs in the DMS (Figures 1G and 5H), the corelease of glutamate from dopamine terminals can facilitate cholinergic transmission in the DMS, but the effect is normally negated by the stronger inhibitory effect of D2 receptors in this region. Blocking group I mGluRs with MPEP (100 μM) and CPCCOEt (100 μM) had no effect on M4-IPSCs in DMS dMSNs (AUC^{-s} post-flash: control, 38.7% ± 7.8% of baseline; antagonists, 45.0% ± 18.4%; p > 0.05, n = 5, Wilcoxon test). However, it eliminated the potentiation of M4-IPSCs in dMSNs in the DLS (AUC^{-s} post-flash: control, 678.3% ± 260.1% of baseline; antagonists, 129.6% ± 21.9%; p < 0.05, n = 6, Wilcoxon test) (Figures 6D and 6E). This suggests that glutamate corelease strongly drives cholinergic transmission in the DLS but has limited effect in the DMS when D2 receptors are not blocked.

Anatomical evidence suggests that dopaminergic terminals form axon-axonal connections with ChIs in the striatum (Chang, 1988). Lastly, to test whether dopamine transmission directly modulates the release of ACh from cholinergic terminals, we performed paired recordings from synaptically connected ChI-dMSN pairs. GIRK2$^+$ dMSNs were recorded in

voltage clamp while ChIs were current-clamped and hyperpolarized to prevent spontaneous firing. Current injections to the ChI with a 750 ms inter-pulse interval triggered two action potentials and drove paired M4-IPSCs in the dMSN. Due to the high probability of ACh release from ChIs onto dMSNs at muscarinic synapses (Mamaligas and Ford, 2016), the second M4-IPSC was depressed relative to the first. The paired-pulse ratio (PPR) of M4-IPSCs was similar between the DMS and the DLS (PPR: DMS, 0.58 ± 0.06, n = 5; 0.56 ± 0.03, n = 6; p > 0.05, Mann-Whitney test) (Figure 7, black), suggesting that the probability of ACh release is similar across regions. To examine how the release of dopamine from SNc terminals regulates the release of ACh, dopamine terminals were optogenetically stimulated 1–1.5 s before triggering action potentials in ChIs. In the DMS, this led to an inhibition in the amplitude of the 1st IPSC and an increase in the PPR (Figures 7A and 7B, blue). The inhibition of ACh release was mediated by activation of D2 receptors, because it was eliminated by sulpiride (500 nM) (PPR: control, 0.58 ± 0.06, n = 5; flash, 0.98 ± 0.07, n = 5; flash + sulpiride, 0.56 ± 0.04, n = 6; control versus flash, p < 0.05; flash versus flash + sulpiride, p < 0.01; control versus flash + sulpiride, p > 0.05; Kruskal-Wallis test) (normalized amplitude of the 1st IPSC: flash, $68.1\% \pm 10.0\%$; flash + sulpiride, $106.1\% \pm 9.4\%$; n = 9; control versus flash, p <0.05; flash versus flash + sulpiride, p < 0.01; Friedman test) (Figures 7A and 7B, purple). In contrast, in the DLS, the amplitude of the 1st IPSC (normalized amplitude: flash, $82.0\% \pm 14.8\%$; flash + sulpiride, $78.3\% \pm 7.5\%$; n = 6; p > 0.05, Friedman test) (Figures 7C and 7D) and PPR of M4-IPSCs was unaffected following the activation of dopamine inputs in either the presence or the absence of sulpiride (PPR: control, 0.56 ± 0.03, n = 6; flash, 0.60 ± 0.11, n = 6; flash + sulpiride, 0.54 ± 0.07, n = 3; p > 0.05; Kruskal-Wallis test) (Figures 7C and 7D). This suggests that phasic activation of dopaminergic inputs inhibits ACh release from ChI terminals through D2 receptors in the DMS, but not in the DLS.

Altogether, these findings revealed that midbrain SNc inputs predominantly inhibit ACh transmission in the DMS via the actions of dopamine but drive ACh transmission in the DLS via the corelease of glutamate.

DISCUSSION

The medial and lateral dorsal striatal sub-regions have differing roles in striatal-dependent associative behaviors, consolidating goal-directed and habitual behaviors, respectively. Dopamine regulates striatal activity throughout dorsal striatal compartments by modulating multiple classes of striatal neurons, including MSNs, GABAergic interneurons, and ChIs (Gerfen and Surmeier, 2011; Kreitzer, 2009). Dopamine input to the DMS and DLS originate from different subsets of SNc neurons that differ functionally and in the motivational signals they encode (Chuhma et al., 2017; Lerner et al., 2015). However, it remains unclear whether this medial-lateral divide also occurs for other striatal neuromodulators and how they may be modulated by dopamine inputs across regions. Here, we found that like dopamine, ACh transmission exhibits regional differences across the dorsal striatum. As a result of increased connectivity and higher basal firing rates, we found that the frequency of cholinergic transmission is higher onto dMSNs in the DMS than the DLS at muscarinic synapses. The long-standing hypothesis of dopamine- ACh balance has depended on the finding that dorsal striatal dopamine inputs inhibit ChI firing through D2

receptor activity (Aosaki et al., 1994b; Chuhma et al., 2014; Maurice et al., 2004; Morris et al., 2004; Schulz and Reynolds, 2013). However, we found that dopamine D2 receptor-mediated inhibition of ChI activity was largely specific to the medial regions of the dorsal striatum. Due to the weaker signaling by D2 receptors in DLS ChIs, the release of dopamine induced only a brief transient inhibition of DLS ChI firing that was rapidly overwhelmed by an mGluR-mediated increase in burst firing as a result of glutamate corelease. Because we found that the level of cholinergic transmission was higher in the DMS than the DLS, our results show that SNc inputs help to partially restore the imbalance of cholinergic transmission across striatal regions by using dopamine to dampen the higher levels in the DMS but glutamate corelease to boost the lower levels in the DLS.

Dopamine neuron-evoked AMPA and NMDA excitatory synaptic events are observed in both MSNs and ChIs of the nucleus accumbens (NAc), but not in the dorsal striatum, indicating that release of glutamate from dopamine neuron terminals occurs primarily in the NAc (Chuhma et al., 2014; Hnasko et al., 2010; Stuber et al., 2010). While activation of dopamine terminals has been found to evoke a depolarizing conductance in ChIs sufficient to transiently increase the baseline firing rate in the dorsal striatum, the underlying mechanisms remained unclear, because it was not blocked by ligand-gated glutamate receptor antagonists (Straub et al., 2014). Here, our data show that glutamate coreleased from dopamine cells directly regulates DLS ChIs via the activation of a group I mGluR-mediated excitatory conductance. Because we found that the resulting inward current was sensitive to chelating intracellular Ca^{2+} with BAPTA, the signaling cascade may involve the activation of phospholipase C (PLC) via G_q-coupled group I mGluRs and the resulting release of Ca^{2+} from intracellular stores. This metabotropic glutamate input was sufficient to drive robust bursts in ChIs (>15-fold increase in frequency) in the DLS. Because application of L-aspartate could equally drive bursting across all ChIs, the weak excitatory effect in the DMS is likely due to limited presynaptic corelease of glutamate in this region. While the application of sulpiride revealed an underlying excitatory mGluR component in the DMS, the excitatory actions of glutamate corelease appear to be limited under basal conditions when D2 receptors are not blocked. Thus, while glutamate corelease can drive cholinergic transmission across the entire dorsal striatum, the effect is greater in the DLS as a result of stronger corelease and limited dopamine D2 receptor-mediated inhibition. However, the molecular mechanisms underlying weaker dopamine D2 signaling lateral ChIs remains unclear and could result from decreased expression of D2 receptors and/or weaker signaling to downstream signaling cascades.

The excitatory input arising from midbrain dopamine neurons differs from the other excitatory inputs from the parafascicular thalamus and motor cortex (Doig et al., 2014; Gerfen, 1992; Matsumoto et al., 2001), because these inputs make excitatory synaptic connections to ChIs at AMPA and NMDA receptor synapses (Ding et al., 2008, 2010; Lapper and Bolam, 1992). Like others (Straub et al., 2014) we found little role for ligand-gated ion channel glutamate receptors in regulating cholinergic excitability. Whether this mGluR-specific input from dopamine cells is a dedicated metabotropic synapse or results from spillover of glutamate from other synapses is not known.

In addition to input activity from dopamine neuron firing, ACh can locally drive dopaminergic transmission in the dorsal striatum and NAc via presynaptic nAChRs on dopamine terminals (Zhou et al., 2001). The synchronous firing of ChIs evokes the release of dopamine directly from dopamine terminals (Cachope et al., 2012; Kress et al., 2014; Mamaligas et al., 2016; Threlfell et al., 2012). Here we found that in the medial region of the striatum, phasic stimulation of dopamine terminals drove a robust inhibition of ChI firing and ACh release. This inhibition of Ach transmission in the DMS could therefore serve as a negative feedback mechanism to restrain subsequent dopamine release driven by presynaptic nicotinic receptors. In contrast, in the DLS, the transient bursts of ChIs by the corelease of glutamate from dopamine terminals may function as a feedforward mechanism to further potentiate dopamine release through these nicotinic receptors. This suggests that striatal ChIs located in different sub-regions can differentially shape the extent of dopaminergic signaling occurring across the dorsal striatum.

ACh provides a powerful influence over striatal output by modulating synaptic inputs to medium spiny neurons though nAChRs, as well as directly regulating their activity and output via muscarinic receptors (Cachope et al., 2012; English et al., 2011; Goldberg et al., 2012; Higley et al., 2009; Mamaligas et al., 2016; Nelson et al., 2014; Threlfell et al., 2012). Through reciprocal interactions with dopamine inputs, ChIs coordinate a balance of dopamine and ACh levels in the striatum. Imbalances in these transmitters are thought to contribute to several striatal-based movement disorders (Aosaki et al., 2010). The regional difference in basal cholinergic transmission across the dorsal striatum and normalization by midbrain inputs may be critical to the balance of these transmitters. This normalizing influence of dopamine neurons may be lost in neurological conditions in which these inputs degenerate, such as Parkinson's disease (PD). The hypercholinergic state that occurs in the striatum of PD patients and animal models could be a consequence of this imbalance. Future work will be needed to see how loss of dopamine neurons drives imbalances in ACh release across striatal regions.

STAR★METHODS

CONTACT FOR REAGENT AND RESOURCE SHARING

Further information and requests for resources and reagents should be directed to and will be fulfilled by the Lead Contact, Christopher P. Ford (christopher.ford@ucdenver.edu).

EXPERIMENTAL MODEL AND SUBJECT DETAILS

Experimental Models—All experiments were approved by and performed in agreement with the guidelines of the Institutional Animal Care and Use Committee (IACUC) at University of Colorado School of Medicine. 6 - 8 week-old mice used in experiments were: DAT[IRES-Cre] heterozygote mice, ChAT[IRES-Cre] heterozygote mice, Ai14 tdTomato reporter mice and wild-type C57BL/6J mice. Both male and female mice were used for all experiments.

Subject Details

Stereotaxic injection: Mice were injected at postnatal day 21. For dorsal striatal injections, 350 nL AAV9.hSynapsin.tdTomato.T2A.mGIRK2-1-A22A.WPRE.bGH (University of Pennsylvania Viral Core) was injected into one hemisphere with the following coordinates (relative to bregma): AP +1.15 mm, ML +1.825 mm, DV −3.325 mm. For SNc injections, 500 nL AAV5.EF1a.DIO.hChR2 (H134R)-EYFP.WPRE.hGH (University of Pennsylvania Viral Core) was injected into the following coordinates (relative to bregma): AP −2.3 mm, ML −1.0 mm, DV −4.7 mm. Virus was injected using a pulled pipette using a Nanoject II (Drummond Scientific). Mice were allowed to recover for at least 3 weeks.

METHOD DETAILS

Slice preparation—Coronal slices (240 μm) containing the dorsal striatum were cut in the ice-cold high sucrose cutting solution containing (in mM): 75 NaCl, 2.5 KCl, 6 $MgCl_2$, 0.1 $CaCl_2$, 1.2 NaH_2PO_4, 25 $NaHCO_3$, 2.5 D-glucose, 50 sucrose and bubbled with 95% O_2 and 5% CO_2. Slices were incubated for 1 h at 32°C in ACSF containing (in mM): 126 NaCl, 2.5 KCl, 1.2 $MgCl_2$, 2.5 $CaCl_2$, 1.2 NaH_2PO_4, 21.4 $NaHCO_3$, 11.1 D-glucose and 10 μM MK-801, and bubbled with 95% O_2 and 5% CO_2. For the experiments examining the effect of NMDA receptors, 1 mM kynurenic acid were added to the cutting solution and slices were incubated in ACSF with no MK-801. Slices were then transferred into a recording chamber and perfused with ACSF (33 ± 2°C) at a rate of 2 mL/min. Neurons were visualized using a BX51WI microscope (Olympus) with an infrared LED (Thorlabs). TdTomato expressing MSNs were visualized with a green LED.

Electrophysiology—All experiments were done in the dorsal striatum. Recordings were made in the striatum using Axopatch 200B amplifiers (Molecular Devices) and acquired using Axograph X (Version 1.6.9) at 10 kHz and filtered to 2 kHz. Glass pipettes were made using a pipette puller (Narishige, PC-10). Pipettes for cell-attached recordings from ChIs contained glucose-free ACSF. Pipettes (~2MΩ) for whole-cell recordings from ChIs contained (in mM): 135 D-gluconic acid (K), 10 HEPES(K), 0.1 $CaCl_2$, 2 $MgCl_2$, 0.1 EGTA. Pipettes (~2MΩ) for MSNs contained (in mM): 115 K-methylsulphate, 20 NaCl, 1.5 $MgCl_2$, 10 HEPES(K), 10 BAPTA-tetrapotassium. All internal solution also contained 0.1 mg/mL GTP, 1 mg/mL ATP, and 1.5 mg/mL phosphocreatine (pH 7.35, 275 mOsm). In all whole-cell recordings, cells were held at −60 mV. No series resistance compensation was applied and cells were discarded if series resistance was over 15 MΩ. Optogenetic stimulation was applied with wide-field blue illumination (2 ms) using a blue LED (470 nm). Dopamine and L-aspartate were iontophoresed using an iontophoresis generator (Dagan). A thin-walled iontophoretic pipette containing dopamine (1M) or L-aspartate (200 mM) was positioned 15~20 μm from the cell. Dopamine was ejected as a cation. A negative 15-20 nA retention current was applied to prevent dopamine leakage in between each pulse. L-aspartate was ejected as an anion and a positive 15-20 nA retention current was applied to prevent leakage.

Evaluation of the firing in ChIs and IPSCs in dMSNs—In cell-attached recordings of ChIs, to describe the average rate of spiking over time, peri-stimulus time histograms of Chis were generated with 200 ms bin size in MATLAB. To evaluate the extent of bursts in

firing, a "burst frequency" was defined as the average firing frequency 0 - 0.5 s post to the first spike after photostimulation. For cluster analysis, Model-based clustering was performed in R using MCLUST (version 5.4, https://cran.r-project.org/web/packages/mclust/index.html). The best model (Gaussian finite mixture model fitted by EM algorithm) for type 2 and 3 ChIs two-dimensional (baseline frequency-burst frequency) clustering was a VVI (diagonal, varying volume and shape) model with 2 clusters, which clearly segregated these two sub-types.

In whole-cell recordings from GIRK$^+$ MSNs, optogenetic stimulation of dopamine terminals also evoked a residual IPSC, which was not fully blocked by D1-receptor antagonists. The average residual IPSC from 15 MSNs, were used to generate a template which was then subtracted from all voltage clamp traces from D1-MSNs to digitally subtract the small residual component. Peri-stimulus time histograms of AUCs were generated with 200 ms bin size in MATLAB.

Connectivity measurments—For calculating the connectivity between ChIs and MSNs, cell-attached recordings were made from ChIs and simultaneous whole-cell recordings were made from synaptically connected GIRK+ MSNs. Recordings (20 s) were acquired and the number of total spontaneous IPSCs and paired spontaneous IPSCs (triggered by APs from the recorded ChIs) were counted. The connectivity was calculated by taking the ratio total IPSCs over the paired IPSCs.

Fluorescence imaging and cell counting—ChAT × Ai14 tdTomato or AAV-ChR2-eYFP-injected DAT$^{IRES-Cre}$ mice were anesthetized with isoflurane and transcardially perfused with 4% paraformaldehyde in PBS containing (in mM): 137 NaCl, 1.5 KH$_2$PO$_4$, 8 NaH$_2$PO$_4$, and 2.7 KCl (pH = 7.4). Brains were post-fixed in 4% PFA for 2 hours and then dehydrated with 30% sucrose in PBS at 4°C overnight. Serial coronal slices (30 μm in thickness) containing the dorsal striatum or the substantia nigra pars compacta were obtained using a cryostat. Fluorescent images were obtained using an Olympus Slide Scanner VS120. ChI counting and image processing were performed in Fiji (ImageJ). For cell counting, the dorsal striatum was hemisected to divide the medial and lateral areas. ChIs were then counted in two ellipses (semi-major axis: 0.5 mm, semi-minor axis: 0.4 mm, close to the dorsal edge) on each side. Since images were obtained using widefield fluorescence through the 30 μm slice tissue, the density of ChIs (/mm^2) may be an overestimate. However, cell counts were done in a similar manner for both the DMS and the DLS in all slices.

Chemicals—Picrotoxin and MK-801 were from Abcam. Sulpiride, SCH23390, CGP55845, DNQX, APV, MPEP, CPCCOEt, clemizole and M 084 were obtained from Tocris Bioscience. K-methylsulfate was obtained from Acros Organic. BAPTA was obtained from Invitrogen. All the other chemicals were from Sigma-Aldrich.

QUANTIFICATION AND STATISTICAL ANALYSIS

All data are shown as mean ± SEM. Statistical tests used for comparisons were non-parametric Mann-Whitney test, Wilcoxon matched-pairs signed rank test, Kruskal-Wallis

test, Friedman test and Pearson's correlations (Prism 7). All the bar graphs and scatterplots represent results from non-parametric statistical tests. The statistical significance was considered as $p < 0.05$ (*), $p < 0.01$ (**), $p < 0.001$ (***) and $p < 0.001$ (****).

Supplementary Material

Refer to Web version on PubMed Central for supplementary material.

ACKNOWLEDGMENTS

REFERENCES

Aosaki T, Tsubokawa H, Ishida A, Watanabe K, Graybiel AM, and Kimura M (1994a). Responses of tonically active neurons in the primate's striatum undergo systematic changes during behavioral sensorimotor conditioning. J. Neurosci 14, 3969–3984. [PubMed: 8207500]

Aosaki T, Graybiel AM, and Kimura M (1994b). Effect of the nigrostriatal dopamine system on acquired neural responses in the striatum of behaving monkeys. Science 265, 412–415. [PubMed: 8023166]

Aosaki T, Kiuchi K, and Kawaguchi Y (1998). Dopamine D1-like receptor activation excites rat striatal large aspiny neurons in vitro. J. Neurosci 18, 5180–5190. [PubMed: 9651201]

Aosaki T, Miura M, Suzuki T, Nishimura K, and Masuda M (2010). Acetylcholine-dopamine balance hypothesis in the striatum: an update. Geriatr. Gerontol. Int 10 (Suppl 1), S148–S157. [PubMed: 20590830]

Berg AP, Sen N, and Bayliss DA (2007). TrpC3/C7 and Slo2.1 are molecular targets for metabotropic glutamate receptor signaling in rat striatal cholinergic interneurons. J. Neurosci 27, 8845–8856. [PubMed: 17699666]

Bergson C, Mrzljak L, Smiley JF, Pappy M, Levenson R, and Goldman-Rakic PS (1995). Regional, cellular, and subcellular variations in the distribution of D1 and D5 dopamine receptors in primate brain. J. Neurosci 15, 7821–7836. [PubMed: 8613722]

Bernard V, Normand E, and Bloch B (1992). Phenotypical characterization of the rat striatal neurons expressing muscarinic receptor genes. J. Neurosci 12, 3591–3600. [PubMed: 1527598]

Bolam JP, Hanley JJ, Booth PA, and Bevan MD (2000). Synaptic organization of the basal ganglia. J. Anat 196, 527–542. [PubMed: 10923985]

Bonsi P, Cuomo D, De Persis C, Centonze D, Bernardi G, Calabresi P, and Pisani A (2005). Modulatory action of metabotropic glutamate receptor (mGluR) 5 on mGluR1 function in striatal cholinergic interneurons. Neuropharmacology 49 (Suppl 1), 104–113. [PubMed: 16005029]

Cachope R, Mateo Y, Mathur BN, Irving J, Wang H-L, Morales M, Lovinger DM, and Cheer JF (2012). Selective activation of cholinergic interneurons enhances accumbal phasic dopamine release: setting the tone for reward processing. Cell Rep. 2, 33–41. [PubMed: 22840394]

Calabresi P, Centonze D, Gubellini P, Pisani A, and Bernardi G (2000). Acetylcholine-mediated modulation of striatal function. Trends Neurosci. 23, 120–126. [PubMed: 10675916]

Chang HT (1988). Dopamine-acetylcholine interaction in the rat striatum: a dual-labeling immunocytochemical study. Brain Res. Bull. 21, 295–304. [PubMed: 2903785]

Chuhma N, Mingote S, Moore H, and Rayport S (2014). Dopamine neurons control striatal cholinergic neurons via regionally heterogeneous dopamine and glutamate signaling. Neuron 81, 901–912. [PubMed: 24559678]

Chuhma N, Mingote S, Kalmbach A, Yetnikoff L, and Rayport S (2017). Heterogeneity in dopamine neuron synaptic actions across the striatum and its relevance for schizophrenia. Biol. Psychiatry 81, 43–51. [PubMed: 27692238]

Devan BD, McDonald RJ, and White NM (1999). Effects of medial and lateral caudate-putamen lesions on place- and cue-guided behaviors in the water maze: relation to thigmotaxis. Behav. Brain Res. 100, 5–14. [PubMed: 10212049]

Ding J, Peterson JD, and Surmeier DJ (2008). Corticostriatal and thalamostriatal synapses have distinctive properties. J. Neurosci 28, 6483–6492. [PubMed: 18562619]

Ding JB, Guzman JN, Peterson JD, Goldberg JA, and Surmeier DJ (2010). Thalamic gating of corticostriatal signaling by cholinergic interneurons. Neuron 67, 294–307. [PubMed: 20670836]

Doig NM, Magill PJ, Apicella P, Bolam JP, and Sharott A (2014). Cortical and thalamic excitation mediate the multiphasic responses of striatal cholinergic interneurons to motivationally salient stimuli. J. Neurosci 34, 3101–3117. [PubMed: 24553950]

El-Hassar L, Hagenston AM, D'Angelo LB, and Yeckel MF (2011). Metabotropic glutamate receptors regulate hippocampal CA1 pyramidal neuron excitability via Ca2+ wave-dependent activation of SK and TRPC channels. J. Physiol 589, 3211–3229. [PubMed: 21576272]

English DF, Ibanez-Sandoval O, Stark E, Tecuapetla F, Buzsa´ ki G, Deisseroth K, Tepper JM, and Koos T. (2011). GABAergic circuits mediate the reinforcement-related signals of striatal cholinergic interneurons. Nat. Neurosci 15, 123–130. [PubMed: 22158514]

Gerfen CR (1992). The neostriatal mosaic: multiple levels of compartmental organization. Trends Neurosci. 15, 133–139. [PubMed: 1374971]

Gerfen CR, and Surmeier DJ (2011). Modulation of striatal projection systems by dopamine. Annu. Rev. Neurosci 34, 441–466. [PubMed: 21469956]

Gerfen CR, and Wilson CJ (1996). The basal ganglia In Handbook of Chemical Neuroanatomy: Integraded Systems of the CNS, Part III: Cerebellum, Basal Ganglia, Olfactory System, Swanson LW, Björklund A, and Hökfelt T, eds. (Elsevier), pp. 371–468.

Goldberg JA, Ding JB, and Surmeier DJ (2012). Muscarinic modulation of striatal function and circuitry. Handb. Exp. Pharmacol 208, 223–241.

Graybiel AM, Aosaki T, Flaherty AW, and Kimura M (1994). The basal ganglia and adaptive motor control. Science 265, 1826–1831. [PubMed: 8091209]

Gremel CM, and Costa RM (2013). Orbitofrontal and striatal circuits dynamically encode the shift between goal-directed and habitual actions. Nat. Commun 4, 2264. [PubMed: 23921250]

Higley MJ, Soler-Llavina GJ, and Sabatini BL (2009). Cholinergic modulation of multivesicular release regulates striatal synaptic potency and integration. Nat. Neurosci 12, 1121–1128. [PubMed: 19668198]

Hnasko TS, Chuhma N, Zhang H, Goh GY, Sulzer D, Palmiter RD, Rayport S, and Edwards RH (2010). Vesicular glutamate transport promotes dopamine storage and glutamate corelease in vivo. Neuron 65, 643–656. [PubMed: 20223200]

Kawaguchi Y (1993). Physiological, morphological, and histochemical characterization of three classes of interneurons in rat neostriatum. J. Neurosci 13, 4908–4923. [PubMed: 7693897]

Kreitzer AC (2009). Physiology and pharmacology of striatal neurons. Annu. Rev. Neurosci 32, 127–147. [PubMed: 19400717]

Kress GJ, Shu H-J, Yu A, Taylor A, Benz A, Harmon S, and Mennerick S (2014). Fast phasic release properties of dopamine studied with a channel biosensor. J. Neurosci 34, 11792–11802. [PubMed: 25164674]

Kupferschmidt DA, Juczewski K, Cui G, Johnson KA, and Lovinger DM (2017). Parallel, but dissociable, processing in discrete corticostriatal inputs encodes skill learning. Neuron 96, 476–489. [PubMed: 29024667]

Lapper SR, and Bolam JP (1992). Input from the frontal cortex and the parafascicular nucleus to cholinergic interneurons in the dorsal striatum of the rat. Neuroscience 51, 533–545. [PubMed: 1488113]

Lerner TN, Shilyansky C, Davidson TJ, Evans KE, Beier KT, Zalocusky KA, Crow AK, Malenka RC, Luo L, Tomer R, and Deisseroth K (2015). Intact-brain analyses reveal distinct information carried by SNc dopamine subcircuits. Cell 162, 635–647. [PubMed: 26232229]

Lim SAO, Kang UJ, and McGehee DS (2014). Striatal cholinergic interneuron regulation and circuit effects. Front. Synaptic Neurosci. 6, 22. [PubMed: 25374536]

Mamaligas AA, and Ford CP (2016). Spontaneous synaptic activation of muscarinic receptors by striatal cholinergic neuron firing. Neuron 91, 574–586. [PubMed: 27373830]

Mamaligas AA, Cai Y, and Ford CP (2016). Nicotinic and opioid receptor regulation of striatal dopamine D2-receptor mediated transmission. Sci. Rep 6, 37834. [PubMed: 27886263]

Marcott PF, Mamaligas AA, and Ford CP (2014). Phasic dopamine release drives rapid activation of striatal D2-receptors. Neuron 84, 164–176. [PubMed: 25242218]

Matsumoto N, Minamimoto T, Graybiel AM, and Kimura M (2001). Neurons in the thalamic CM-Pf complex supply striatal neurons with information about behaviorally significant sensory events. J. Neurophysiol 85, 960–976. [PubMed: 11160526]

Maurice N, Mercer J, Chan CS, Hernandez-Lopez S, Held J, Tkatch T, and Surmeier DJ (2004). D2 dopamine receptor-mediated modulation of voltage-dependent Na+ channels reduces autonomous activity in striatal cholinergic interneurons. J. Neurosci 24, 10289–10301. [PubMed: 15548642]

McGeorge AJ, and Faull RLM (1989). The organization of the projection from the cerebral cortex to the striatum in the rat. Neuroscience 29, 503–537. [PubMed: 2472578]

Morris G, Arkadir D, Nevet A, Vaadia E, and Bergman H (2004). Coincident but distinct messages of midbrain dopamine and striatal tonically active neurons. Neuron 43, 133–143. [PubMed: 15233923]

Nelson AB, Hammack N, Yang CF, Shah NM, Seal RP, and Kreitzer AC (2014). Striatal cholinergic interneurons drive GABA release from dopamine terminals. Neuron 82, 63–70. [PubMed: 24613418]

Pisani A, Bonsi P, Centonze D, Bernardi G, and Calabresi P (2001). Functional coexpression of excitatory mGluR1 and mGluR5 on striatal cholinergic interneurons. Neuropharmacology 40, 460–463. [PubMed: 11166340]

Pisani A, Bernardi G, Ding J, and Surmeier DJ (2007). Re-emergence of striatal cholinergic interneurons in movement disorders. Trends Neurosci. 30, 545–553. [PubMed: 17904652]

Schulz JM, and Reynolds JNJ (2013). Pause and rebound: sensory control of cholinergic signaling in the striatum. Trends Neurosci. 36, 41–50. [PubMed: 23073210]

Straub C, Tritsch NX, Hagan NA, Gu C, and Sabatini BL (2014). Multiphasic modulation of cholinergic interneurons by nigrostriatal afferents. J. Neurosci 34, 8557–8569. [PubMed: 24948810]

Stuber GD, Hnasko TS, Britt JP, Edwards RH, and Bonci A (2010). Dopaminergic terminals in the nucleus accumbens but not the dorsal striatum corelease glutamate. J. Neurosci 30, 8229–8233. [PubMed: 20554874]

Tallaksen-Greene SJ, Kaatz KW, Romano C, and Albin RL (1998). Localization of mGluR1a-like immunoreactivity and mGluR5-like immunoreactivity in identified populations of striatal neurons. Brain Res. 780, 210–217. [PubMed: 9507137]

Threlfell S, Lalic T, Platt NJ, Jennings KA, Deisseroth K, and Cragg SJ (2012). Striatal dopamine release is triggered by synchronized activity in cholinergic interneurons. Neuron 75, 58–64. [PubMed: 22794260]

Tritsch NX, Ding JB, and Sabatini BL (2012). Dopaminergic neurons inhibit striatal output through non-canonical release of GABA. Nature 490, 262–266. [PubMed: 23034651]

West MO, Carelli RM, Pomerantz M, Cohen SM, Gardner JP, Chapin JK, and Woodward DJ (1990). A region in the dorsolateral striatum of the rat exhibiting single-unit correlations with specific locomotor limb movements. J. Neurophysiol 64, 1233–1246. [PubMed: 2258744]

Yan Z, and Surmeier DJ (1997). D5 dopamine receptors enhance Zn2+-sensitive GABA(A) currents in striatal cholinergic interneurons through a PKA/PP1 cascade. Neuron 19, 1115–1126. [PubMed: 9390524]

Yan Z, Flores-Hernandez J, and Surmeier DJ (2001). Coordinated expression of muscarinic receptor messenger RNAs in striatal medium spiny neurons. Neuroscience 103, 1017–1024. [PubMed: 11301208]

Yin HH, and Knowlton BJ (2006). The role of the basal ganglia in habit formation. Nat. Rev. Neurosci 7, 464–476. [PubMed: 16715055]

Yin HH, Knowlton BJ, and Balleine BW (2004). Lesions of dorsolateral striatum preserve outcome expectancy but disrupt habit formation in instrumental learning. Eur. J. Neurosci 19, 181–189. [PubMed: 14750976]

Yin HH, Ostlund SB, Knowlton BJ, and Balleine BW (2005). The role of the dorsomedial striatum in instrumental conditioning. Eur. J. Neurosci 22, 513–523. [PubMed: 16045504]

Zhou FM, Liang Y, and Dani JA (2001). Endogenous nicotinic cholinergic activity regulates dopamine release in the striatum. Nat. Neurosci 4, 1224–1229. [PubMed: 11713470]

Highlights

- The frequency of cholinergic transmission onto dMSNs is higher in the DMS than the DLS

- SNc inputs drive pauses in DMS cholinergic interneurons via D2 receptors

- SNc inputs drive bursts in DLS cholinergic interneurons via mGluR receptors

- DA cells differentially modulate ChIs to maintain constant ACh release across areas
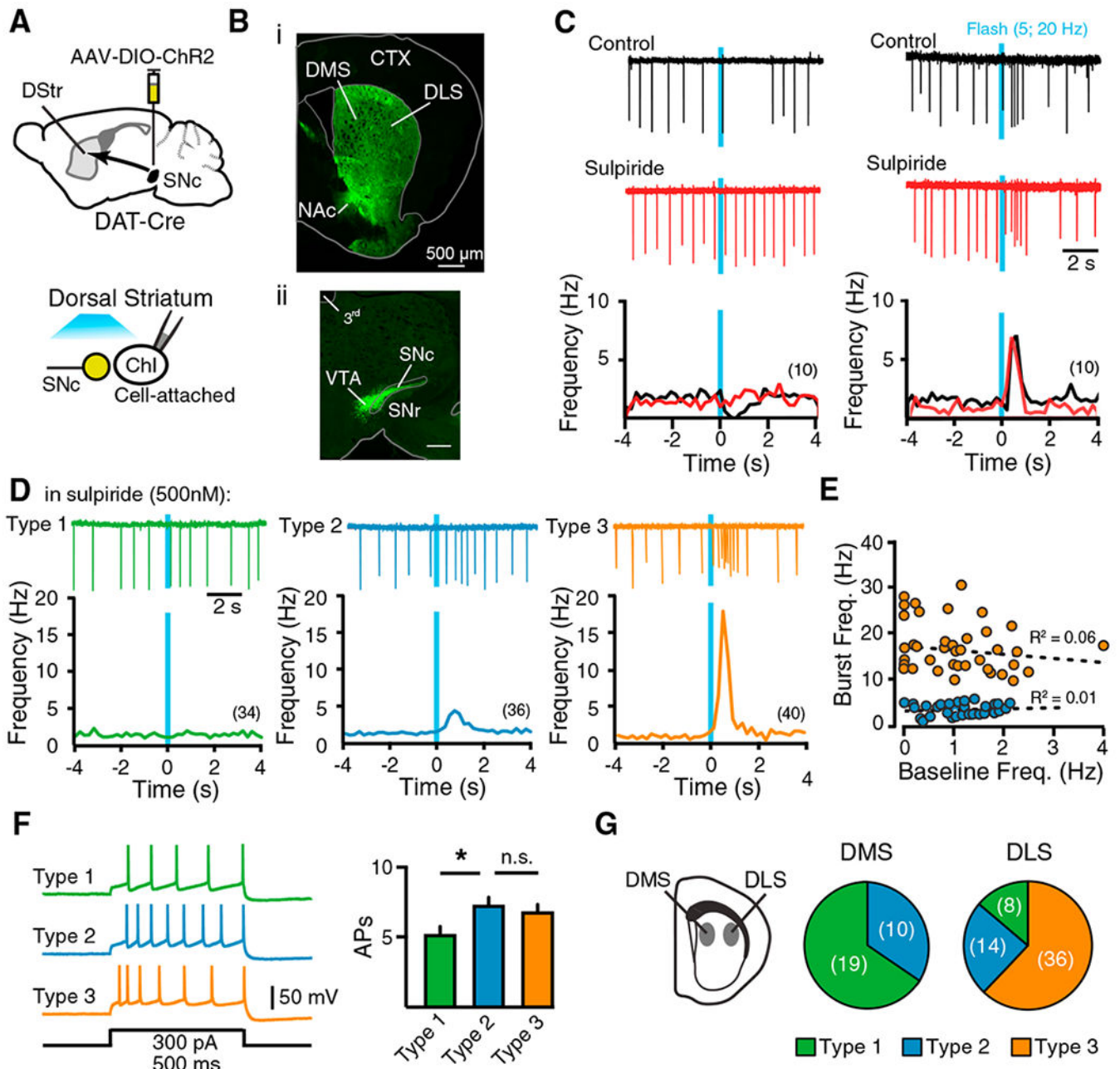
Figure 1. Midbrain Dopamine Inputs Differentially Regulate DMS and DLS ChIs

(A) Schematic of AAV injection and recording condition.

(B) Widefield images showing the fluorescence of EYFP. (i) Image of coronal striatal section from a DAT-Cre mouse injected with AAV-ChR2-EYFP in the midbrain. (ii) Image showing the SNc and ventral tegmental area (VTA) from a DAT-Cre mouse injected with AAV-ChR2-EYFP in the midbrain.

(C) Example traces of cell-attached recordings from control cholinergic interneurons (ChIs) (top, black) in the presence of sulpiride (middle, red) and the population peristimulus histograms. Bin size: 200 ms.

(D) Representative traces of ChI types (top) and population peristimulus histograms. Bin size: 200 ms.

(E) Correlation of burst frequency against baseline frequency of all type 2 (blue circles) and 3 (orange circles) ChIs.

(F) Example traces and summary of evoked action potentials from type 1, type 2, and type 3 ChIs.

(G) Proportion of type 1, type 2, and type 3 ChIs in the dorsomedial striatum (DMS) or dorsolateral striatum (DLS).
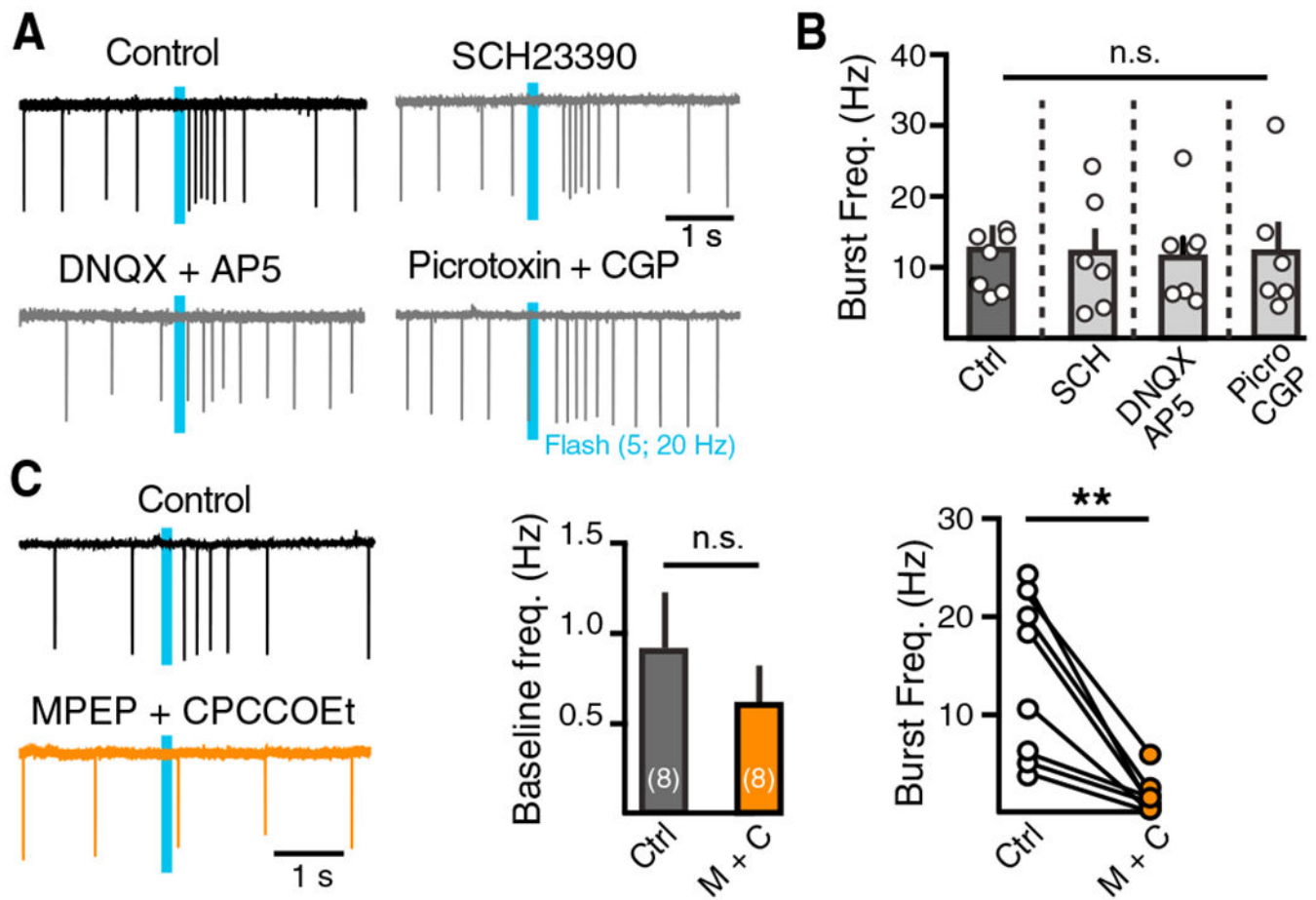
Summary data are mean ± SEM. *p < 0.05.

Figure 2. Striatal Dopamine Inputs Drive ChI Burst Firing through mGluRs

(A) Representative traces from ChIs showing optogenetically evoked burst response in control, presence of picrotoxin (100 μM) + CGP55845 (300 nM), DNQX (10 μM) + AP5 (10 μM), or SCH23390 (1 μM).

(B) Summary of pharmacological data.

(C) Group 1 mGluR antagonists MPEP (100 μM) and CPCCOEt (100 μM) block dopamine neuron-induced ChI burst firing.
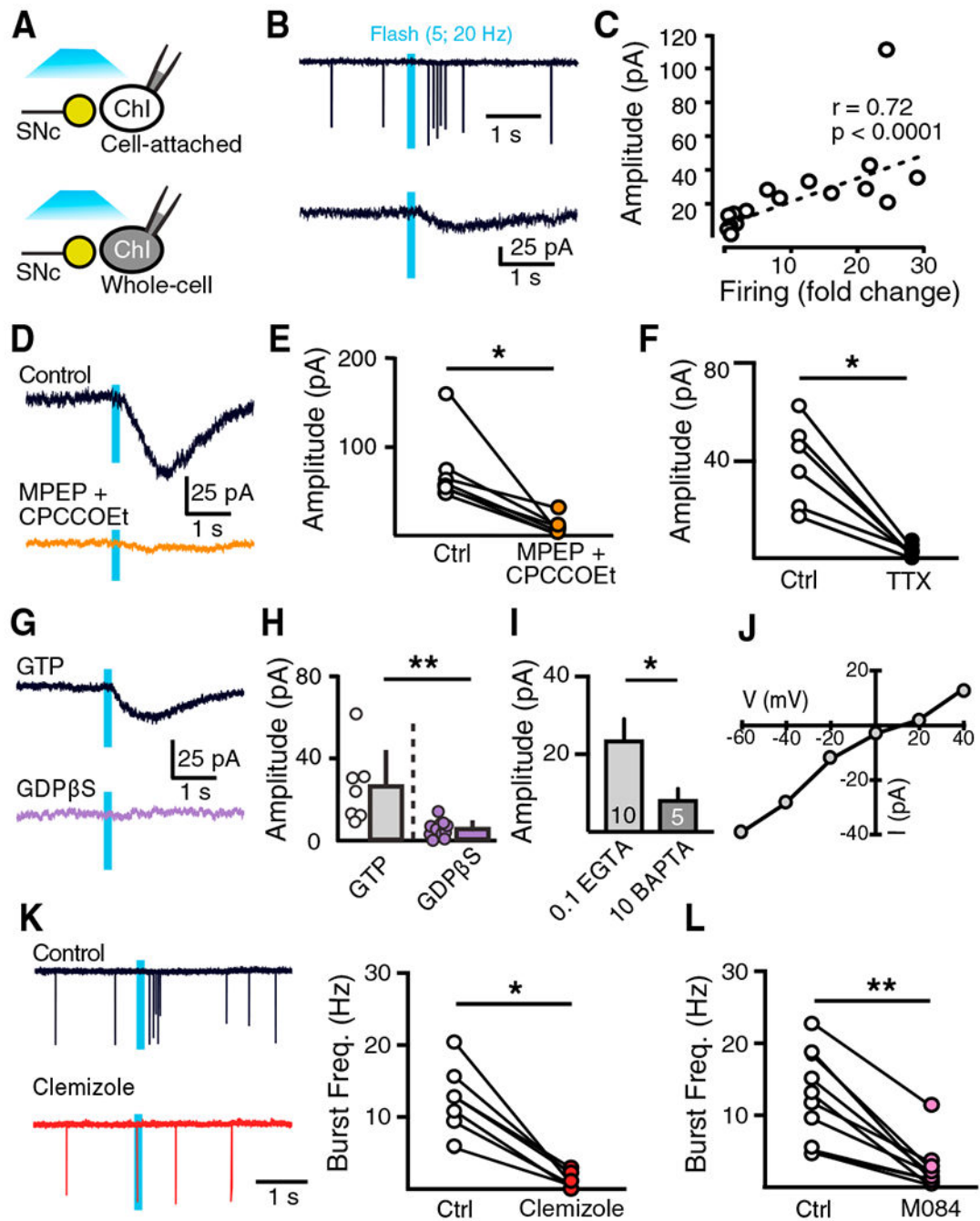
Error bars represent SEM. *p < 0.05, **p < 0.01.

Figure 3. mGluR-Mediated Excitatory Conductance Drives Burst Firing in ChIs

(A) Schematic of the recording condition. Cell-attached and whole-cell voltage-clamp recordings were sequentially made from the same ChI.

(B) Representative traces from the same ChI under cell-attached mode (top) and voltage-clamp mode (bottom) following dopamine photoactivation.

(C) Linear regression between fold change of firing (burst frequency divided by baseline frequency) and inward current amplitude.

(D) Representative traces with mGluR1 antagonist MPEP (100 μM) and CPCCOEt (100 μM).

(E) Summary of inward current amplitudes with MPEP and CPCCOEt.

(F) Summary of the effect of TTX (200 nM) on inward current amplitudes in ChIs.

(G) Representative traces of dopamine input-driven inward currents in ChI with intracellular guanosine triphosphate (GTP) or GDPβS.

(H) Summary of the inward current amplitudes with GTP or GDPβS.

(I)Summary of inward current amplitudes with 0.1 mM EGTA and 10 mM BAPTA.

(J) Current-voltage (I-V) relationship of the dopamine-induced inward current.

(K) Representative traces and summary data in the presence of clemizole (10 μM).

(L) Summary of burst frequencies in M 084 (100 μM).

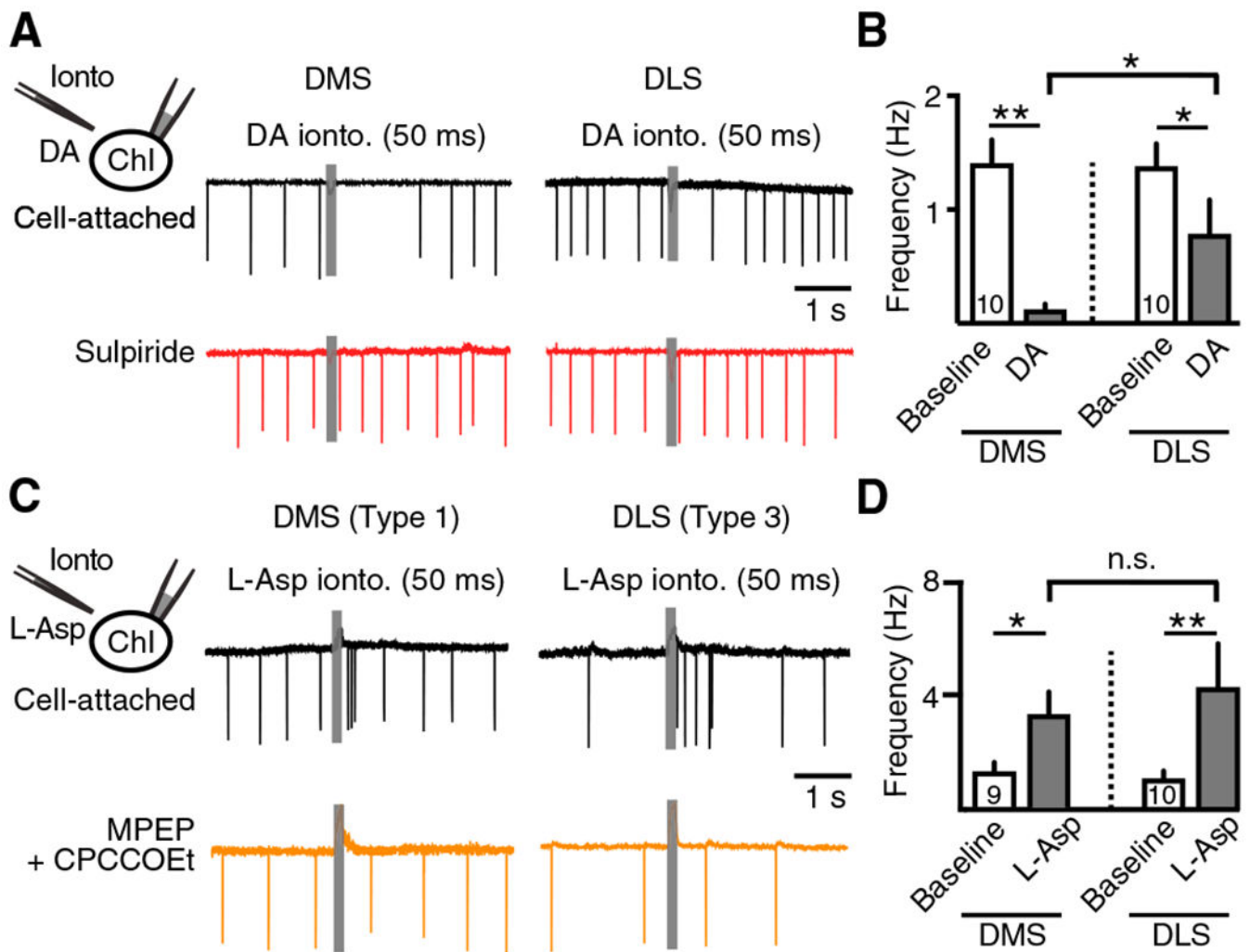Error bars represent SEM. *p < 0.05, **p < 0.01.

Figure 4. Post-synaptic Responses of DMS and DLS ChIs in Response to Iontophoretic Application of Dopamine or L-aspartate

(A) Sample traces of cell-attached recordings from DMS and DLS ChIs in response to iontophoretic application of dopamine (1 M, 50 ms).

(B) Quantification of the dopamine-induced decrease in firing in DMS and DLS ChIs.

(C) Sample traces of cell-attached recordings from a type 1 DMS ChI and a type 3 DLS ChI in response to iontophoretic application of L-aspartate (200 mM, 50 ms).

(D) Quantification of the L-aspartate-induced increase in firing in DMS and DLS ChIs.

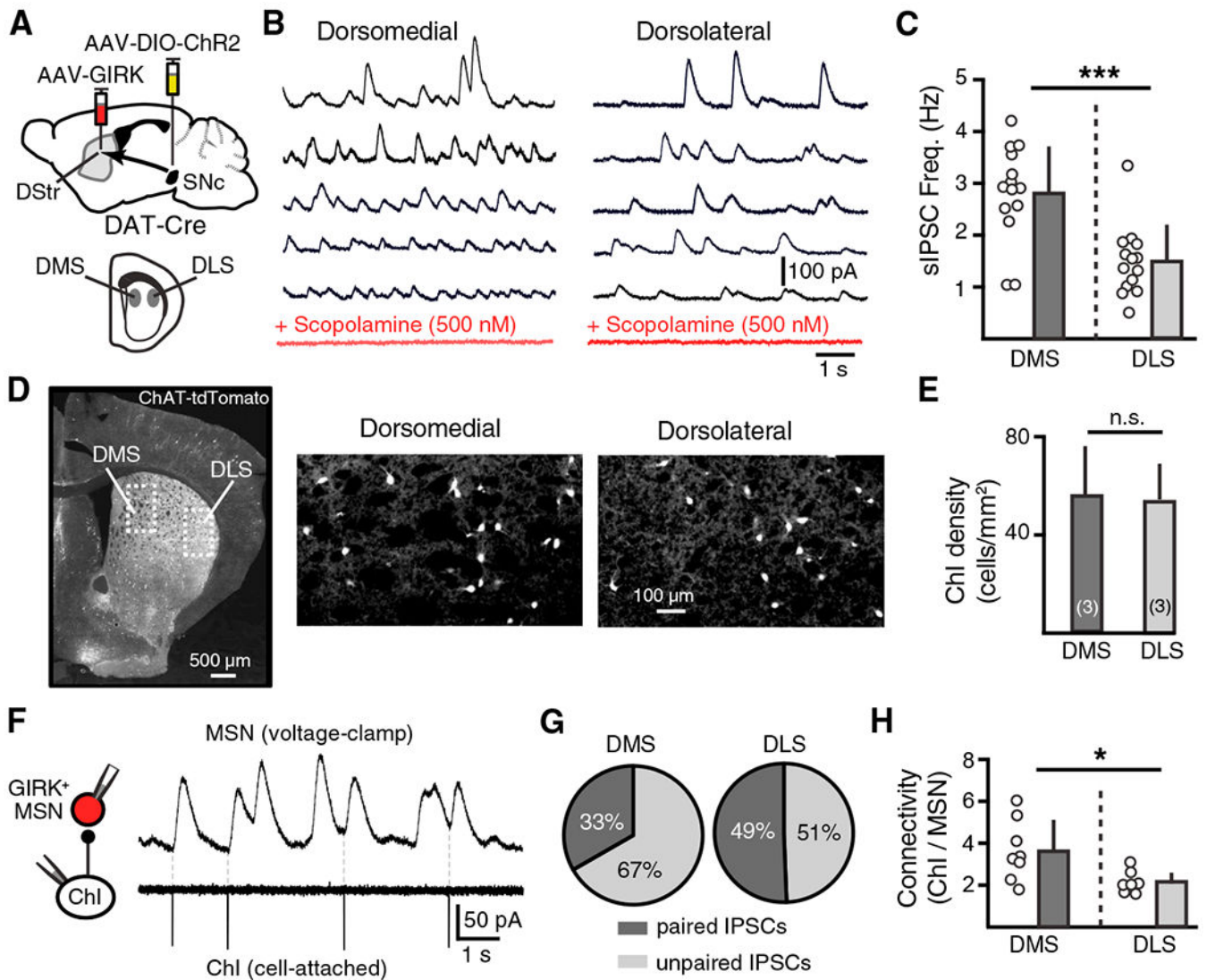Error bars represent SEM. $*p < 0.05$, $**p < 0.01$.

Figure 5. Regional Differences in Cholinergic Transmission and Connectivity between ChIs and dMSNs at Muscarinic Synapses

(A) Schematic of injection of AAV-GIRK2-tdTomato to the dorsal striatum and AAV-DIO-ChR2 to the midbrain of DAT-Cre mice.

(B) M4-sIPSCs from GIRK2$^+$ (Kir$_{3.2}$$^+$) dMSNs in the DMS and DLS in the control condition (black) and in scopolamine (500 nM, red).

(C) Summary M4-sIPSC frequencies in DMS and DLS dMSNs.

(D) Left: widefield image of the coronal striatal section from Chat-tdTomato mice showing tdTomato fluorescence. Right: zoomed in view of the inset for DMS and DLS.

(E) ChI densities (number of ChIs per square millimeter) in the DMS or DLS as counted by widefield fluorescence.

(F) Representative traces of paired recordings showing APs in the ChI trigger time-locked (paired) IPSCs in the paired MSN.

(G) Averaged percentage of paired and unpaired IPSCs in one ChI-MSN pair in the DMS or DLS.

(H) Connectivity of ChIs to MSNs, illustrating the number of ChIs connected to one dMSN in the DMS or DLS.

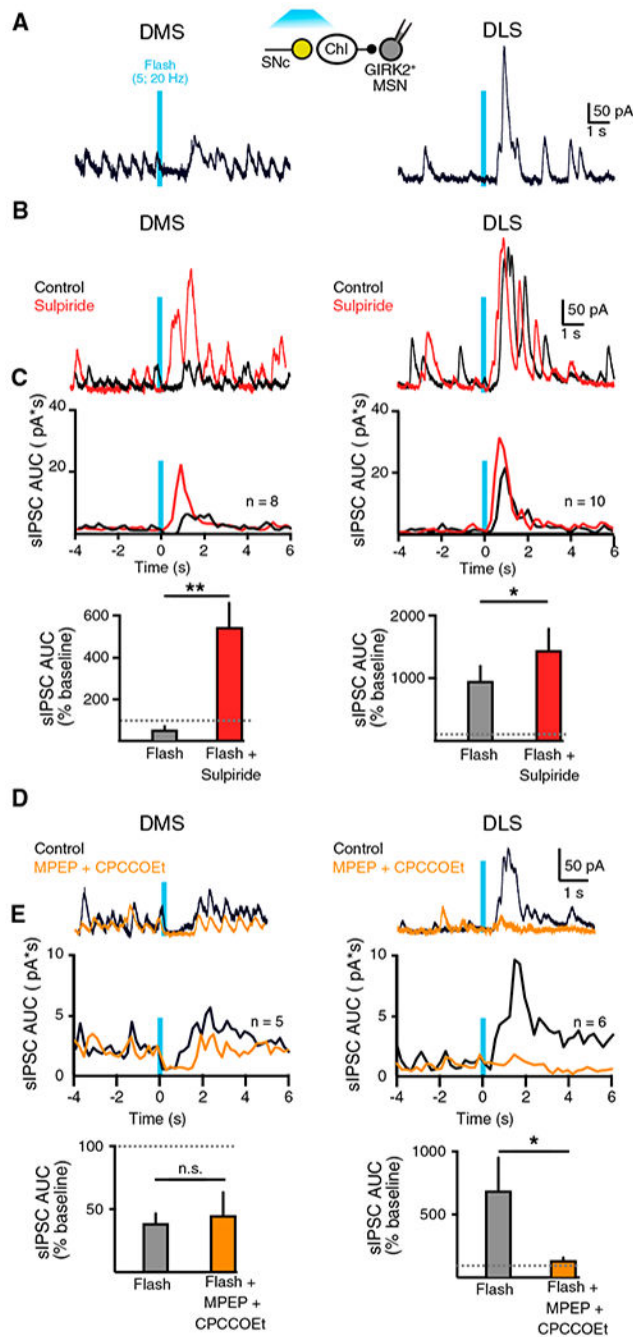Error bars represent SEM. *p < 0.05, ***p < 0.001.

Figure 6. Dopamine Inputs Balance Cholinergic Transmission across the Striatum

(A) Whole-cell recordings from GIRK⁺ dMSNs in the DMS (left) or in the DLS (right) following photostimulation of dopamine inputs.

(B) Example traces of showing the effect of sulpiride (500 nM) on evoked M4-IPSCs in the DMS or DLS dMSNs. Black, in control condition; red, in sulpiride.

(C) Top: peristimulustime histograms (bin size: 200 ms) quantifying the AUCs for M4-sIPSC. Bottom: Summary of the AUCs of M4-sIPSCs 2 s following stimulation of dopamine terminals in the DMS and DLS. Black, control; red, sulpiride.

(D) Whole-cell recordings from GIRK$^+$ dMSNs in the DMS (left) or in the DLS (right) following photostimulation of dopamine inputs in control (black) or MPEP and CPCCOEt (orange).

(E) Top: peristimulus time histograms (bin size: 200 ms) quantifying the AUCs for M4-sIPSC. Bottom: summary of the AUCs of M4-sIPSCs 2 s following stimulation of dopamine terminals in the DMS and DLS. Black, control; orange, MPEP and CPCCOEt.

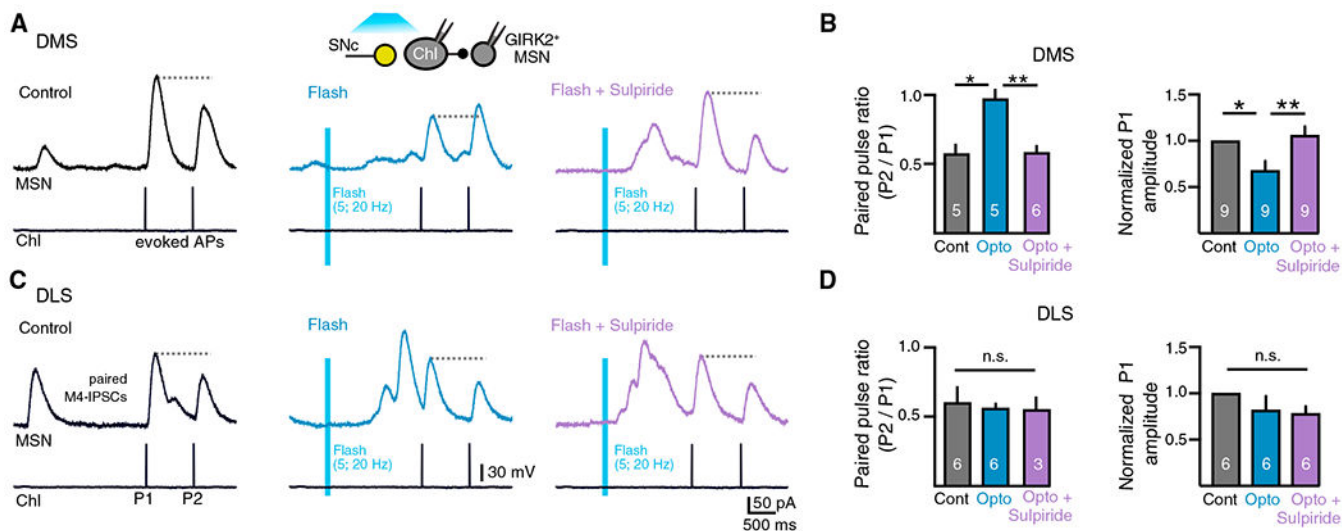Summary data are mean ± SEM. *p < 0.05, **p < 0.01.

Figure 7. Dopamine Inputs Inhibit Acetylcholine Release at Muscarinic Synapses Only in the DMS

(A) Paired recordings made from ChI-dMSN pairs in the DMS. A pair of evoked action potentials in control condition (black) and paired IPSCs evoked 1.5 s after photostimulation of dopamine terminals (flash, blue) and in the presence of sulpiride (500 nM, flash + sulpiride, purple). ChIs hyperpolarized to prevent firing except when triggered. Inter-pulse interval P1 to P2 is 750 ms.

(B) Left: quantification of paired-pulse ratios of paired IPSCs for the paired recordings represented in (A). Right: normalized amplitude of paired M4-IPSCs under control conditions (black), following photoactivation of SNc dopamine terminals (flash, blue) or following photoactivation of SNc dopamine terminals in the presence of sulpiride (500 nM) (flash + sulpiride, purple) from the DMS.

(C) Left: paired recordings are made from ChI-dMSN pairs in the DLS.

(D) Quantification of paired-pulse ratios of paired IPSCs for the paired recordings represented in (C). Right: normalized amplitude of paired M4-IPSCs under control conditions (black), following photoactivation of SNc dopamine terminals (flash, blue) or following photoactivation of SNc dopamine terminals in the presence of sulpiride (500 nM) (flash + sulpiride, purple) from the DLS.

Error bars represent SEM. *p < 0.05, **p < 0.01.

KEY RESOURCES TABLE

REAGENT or RESOURCE	SOURCE	IDENTIFIER
Bacterial and Virus Strains		
AAV9.hSynapsin.tdTomato.T2A.mGIRK2-1-A22A.WPRE	University of Pennsylvania Viral Core	V3992MI-R
AAV5.EF1a. DIO.hChR2(H134R)-EYFP.WPRE.hGH	University of Pennsylvania Viral Core	AV-5-20298P
Chemicals, Peptides, and Recombinant Proteins		
D-Aspartic acid	Tocris	Cat #0213
D-AP5	Tocris	Cat #0106
CGP55845	Tocris	Cat# 1248
Clemizole hydrochloride	Tocris	Cat # 5371
CPCCOEt	Tocris	Cat# 1028
DNQX	Tocris	Cat #0189
Dopamine hydrochloride	Sigma-Aldrich	Cat # H8502
M 084 hydrochloride	Tocris	Cat # 5807
MK-801	Tocris	Cat # 0924
MPEP hydrochloride	Tocris	Cat# 1212
Picrotoxin	Tocris	Cat# 1128
SCH23390	Tocris	Cat 0925
Scopolamine hydrobromide	Tocris	Cat# 1414
Tetrodotoxin	Tocris	Cat# 1078
Experimental Models: Organisms/Strains		
C57BL/6J	Jackson Labs	Stock # 000664
B6;129S6-Gt(ROSA)26Sortm14(CAG-tdTomato)Hze/J	Jackson Labs	Stock # 007908
DAT-IRES-cre B6.SJL-slc6a3tm1.1(cre)bkmn/J	Jackson Labs	Stock # 006660
B6;129S6-Chattm2(cre)Lowl/J	Jackson Labs	Stock # 006410
Software and Algorithms		
Axograph X	Axograph Scientific	https://axograph.com
MATLAB_R2017b	MathWorks	https://www.mathworks.com
Prism 7	Graphpad Software	https://www.graphpad.com/
R studio	RStudio, Inc.	https://www.rstudio.com/